Results in Engineering 18 (2023) 101164

Contents lists available at ScienceDirect

Results in Engineering

journal homepage: www.sciencedirect.com/journal/results-in-engineering

Multimetal removal in aqueous medium using a potato starch/nopal mucilage copolymer: A study of adsorption kinetics and isotherms

David Choque-Quispe [a,b,c,d,*], Carlos A. Ligarda-Samanez [b,c,d,e], Yudith Choque-Quispe [a,c,d,f], Aydeé M. Solano-Reynoso [c,d,g], Betsy S. Ramos-Pacheco [a,b,c,d], Miluska M. Zamalloa-Puma [h], Genaro Julio Álvarez-López [i], Alan Zamalloa-Puma [h], Katya Choque-Quispe [j], Humberto Alzamora-Flores [k]

[a] Water and Food Treatment Materials Research Laboratory, Universidad Nacional José María Arguedas, Andahuaylas, 03701, Peru
[b] Department of Agroindustrial Engineering, Universidad Nacional José María Arguedas, Andahuaylas, 03701, Peru
[c] Research Group in the Development of Advanced Materials for Water and Food Treatment, Universidad Nacional José María Arguedas, Andahuaylas, 03701, Peru
[d] Nutraceuticals and Biopolymers Research Group, Universidad Nacional José María Arguedas, Andahuaylas, 03701, Peru
[e] Food Nanotechnology Research Laboratory, Universidad Nacional José María Arguedas, Andahuaylas, 03701, Peru
[f] Department of Environmental Engineering, Universidad Nacional José María Arguedas, Andahuaylas, 03701, Peru
[g] Department of Basic Sciences, Universidad Nacional José María Arguedas, Andahuaylas, 03701, Peru
[h] Department of Physics, Universidad Nacional de San Antonio Abad Del Cusco, Cusco, 08000, Peru
[i] Law and Humanities Faculty, Universidad Continental, Cusco, 08000, Peru
[j] Universidad Nacional de San Antonio Abad Del Cusco, Cusco, 08000, Peru
[k] Education Deparment, Universidad Nacional de San Antonio Abad Del Cusco, Cusco, 08000, Peru

ARTICLE INFO

Keywords:
Adsorption isotherms
Adsorption kinetics
Native potato starch
Nopal mucilage
Multimetal aqueous system

ABSTRACT

In reducing heavy metals from water for direct or indirect consumption, various synthetic materials have been used; there is a tendency to use natural, biodegradable, and environmentally friendly materials. The aim was to elaborate copolymers with native potato starch and cactus mucilage and evaluate water's multimetal removal capacity. The copolymer was characterized, and the kinetics and adsorption isotherms were evaluated. The copolymers presented high solubility for nopal mucilage levels of 5% w/w, with particle size in aqueous solution less than 422.83 nm, zero charge point around pH 5.5, and potential ζ between −16.72 and −29.80 mV; FTIR analysis showed the predominance of anionic groups with chelating capacity. Multimetal adsorption was from 102.20 to 151.43 mg/g, with affinity in the order Pb > As > Al > Hg > Cr, being higher at pH 6 (p-value<0.05). Kinetic data were fitted to the PSFO, PSSO, and Elovich models with R^2>0.994, X^2<16.098, ARE<34.038, and random residual dispersion, indicating a chemisorption process. The adsorption isotherms were adjusted to the Langmuir, Freundlich, and Redlich-Peterson models with R^2>0.863, whose parameters are related to the ionic radius of the metals, with favorable adsorption and a heterogeneous surface of the copolymer. The mean adsorption energy was found between 0.05 and 0.23 kJ/mol. The use of native potato starch and cactus mucilage allows the formulation of copolymers with high multimetal adsorption potential in aqueous systems.

1. Introduction

Extractive activities, concentration, and refining of metallic minerals are developed in the high Andean areas of South America, whose metallic materials are constituted mainly of copper, gold, silver, zinc, and iron. These metals are mineralized with considerable amounts of metals heavy as lead, arsenic, chromium, mercury, and cadmium, among others [1]. Informal and illegal mining in these extractive areas does not establish adequate management of minerals during exploitation, causing a negative impact on the surrounding environment [2].

Water use during extractive mining activities is indispensable, as well as surfactant, foaming, and acid substances, whose residues generate mine tailings. Moreover, soil removal exposes the minerals to leaching by the action of heavy rains [3,4]. Both tailings and mine leachate can infiltrate the groundwater table and transport dissolved metal ions, which could emerge in water sources such as springs [5].

* Corresponding author. Water and Food Treatment Materials Research Laboratory, Universidad Nacional José María Arguedas, Andahuaylas, 03701, Peru.
E-mail address: dchoque@unajma.edu.pe (D. Choque-Quispe).

https://doi.org/10.1016/j.rineng.2023.101164
Received 30 March 2023; Received in revised form 6 May 2023; Accepted 11 May 2023
Available online 12 May 2023

Table 1
Formulation of the copolymers.

Formulation	SS (%, w/w)	MS (%, w/w)	G (%, w/w)
F1	93.00	5.00	2.00
F2	91.00	4.00	5.00
F3	90.00	5.00	5.00
F4	94.00	3.00	3.00

Likewise, water for human consumption can be collected from springs, which have qualities that depend on the geomorphology of the basin to which they belong and may contain levels of heavy metals that are harmful to human health [5,6].

Developed and developing countries show great concern for providing safe drinking water, especially water containing levels of heavy metals below the maximum permissible limits, according to the regulations of each country [7,8]. Different technologies have been developed to treat water and guarantee its consumption, including chemical, physical, and combined treatments.

The use of biodegradable materials, such as cellulosic residues, starches, and activated proteins, and non-degradable ones, such as activated carbon, activated clays, and ionic polymer resins, have gained momentum in recent years, these materials present high selectivity for heavy metals, allowing removal of up to 99% in concentrations lower than 10 ppm in water with unimetal and multimetal content [9–13]. Likewise, it has been observed that these materials present high efficiency in the removal of other emerging polluting substances in wastewater and natural waters [14,15].

The removal of heavy metals by the action of materials of biological origin is manifested by chemisorption due to the availability of anionic functional groups such as hydroxyl, carbonyl, and carboxyl [16–18] or the establishment of intermolecular forces, and electrostatic attraction that leads to physisorption processes [19,20]. The ability of a material to adsorb metals will depend on improving these processes, which can be achieved through the activation of adsorbent materials with different treatments or the synergy of two or more constituents [20–22].

The use of potato starch (*Solanum tuberosum*) as an adsorbent medium has been widely used in the removal of heavy metals [21,23–25], in the same way, nopal and its mucilage (*Opuntia ficus indica*) [26,27], both polysaccharides offer anionic groups that constitute the active site, with high affinity for cationic species such as heavy metals. The synergy of these two materials can be an alternative to generating a copolymer; however, knowing how fast the material adsorbs and saturates will allow its employability, which could be known through studying the kinetics and adsorption isotherms.

The research aimed to evaluate a copolymer's kinetics and adsorption isotherms elaborated with native potato starch/nopal mucilage. The copolymer was characterized through ζ potential, particle size, FTIR analysis, and zero charge point to achieve this purpose. Likewise, the effect of pH, contact time, and copolymer dose were evaluated to know the parameters of the kinetic and adsorption isotherms.

2. Materials and methods

2.1. Raw material and reagents

Native potato variety Allca Sipas (*Solanum tuberosum* ssp andigenum) and nopal cladodes (*Opuntia ficus* indica), were collected from the cultivated fields of the Huancas Populated Center, Andahuaylas, Peru (13°40′42″S, 73° 15′11″W, and 3742 m of altitude), in the vegetative period from October 2020 to March 2021.

Chemical substances were used, such as glycerin (99% purity, food grade) from the Scharlau brand (Spain); ionic solution of Al, As, Cr, Hg, and Pb for ICP-OES of the SCP SCIENCE brand (Quebec, QC, Canada), and potassium bromide (IR Grade) of the Merck brand (Darmstadt, Germany).

2.2. Starch and nopal mucilage extraction

The starch was obtained by aqueous extraction from the native potato of the Alcca sipas variety and dried at 45 ± 2 °C for 14 h, then the size was reduced in a Resch PM10 planetary ball mill (Haan, Germany), at 150 rpm for 3 min and sieved to < 52 μm in a Resch model AS 200 sieve (Haan, Germany).

The mucilage was obtained by chopping the nopal cladodes, immersing them in distilled water in a 1:1 ratio, and kept at 4 °C. After 24 h, the obtained liquid was treated with 96% ethanol, in a 3:1 ratio to extract the precipitated mucilage, and dried at 70 °C for 24 h Then it was ground to <52 μm in a planetary ball mill at 150 rpm for 3 min.

2.3. Copolymer formulation

A 2% w/v aqueous solution of starch (SS) and 0.5% w/v dehydrated mucilage (MS) was prepared; both solutions were mixed at 50 °C in the order *SS*-G-MS, under continuous agitation for 10 min according to the formulations in Table 1. The samples were then placed in molds and dried at 60 °C for 24 h in a forced convection dryer, Binder model FED (Tuttlingen, Germany). The sequence is shown in Fig. 1.

Where: F, formulation; SS, starch solution; MS, mucilage solution; G, glycerin.

2.4. Solubility determination

The copolymer was previously dried at 105 °C for 24 h to determine the initial weight of the dry material, and it was allowed to cool in a desiccator with excess silica. A sample was dissolved in an aqueous medium at pH 5, 7, and 8, in a ratio of 1/100 (g/mL); it was left stirring at 40 rpm for 24 h and 25 °C, and the glass containers that contained them were sealed to prevent water evaporation. The disintegrated fraction was passed through filter paper and dried at 105 °C for 24 h. The solubility was expressed in terms of the percentage of dry material disintegrated [28,29].

2.5. Zero charge point determination

Solutions were prepared at pH 2, 3, 4, 5, 6, 7, 8, 9, 10, and 12, adjusted with 0.1 N NaOH and 0.1 N HCl. Added 0.05 g of the copolymer to 50 mL of each solution, and it was taken to continuous agitation at 150 rpm for 24 h at room temperature. In the end, the pH of the resulting solution was measured [18].

To find the ZCP, the initial pH and the solution's final pH values were plotted, and the intersection between the curves reports the ZCP value.

2.6. Determination of particle size and ζ potential of the copolymer

0.10 g of the copolymer was taken and placed in 100 mL of ultrapure water for 24 h, continuously stirring at 200 rpm, then placed in a Sonics model VCX 750 (Newtown, CT, USA) sonicator for 10 min at room temperature. An aliquot was taken in a polystyrene cell, and the particle size distribution was determined by dynamic light scattering (DLS) in a Malvern brand equipment, model Zetasizer ZSU3100 (Worcestershire, WR, UK). In the same way, an aliquot was taken and placed in the model DTS1070 folded capillary cell to determine the ζ potential.

2.7. FTIR analysis of the copolymer

0.1% copolymer tablets were prepared with KBr (IR Grade, Darmstadt, Germany). They were taken to the transmission module of the FTIR spectrometer (Fourier-transform infrared spectroscopy), Thermo Fisher (Waltham, MA, USA), Nicolet IS50 model, in a range of 4000–400 cm^{-1} with a resolution of 4 cm^{-1}.

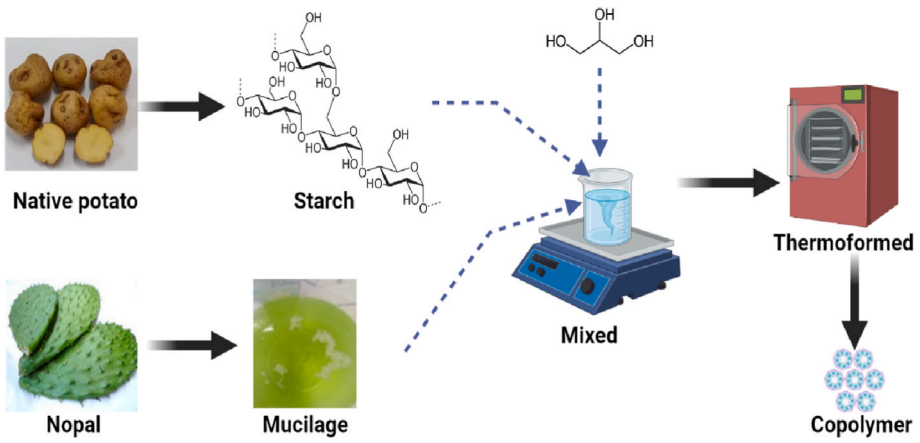

Fig. 1. Copolymer preparation diagram.

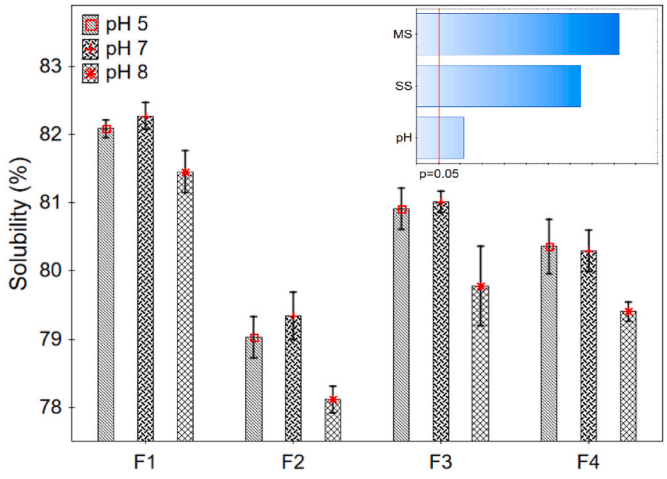

Fig. 2. Solubility of the copolymers.

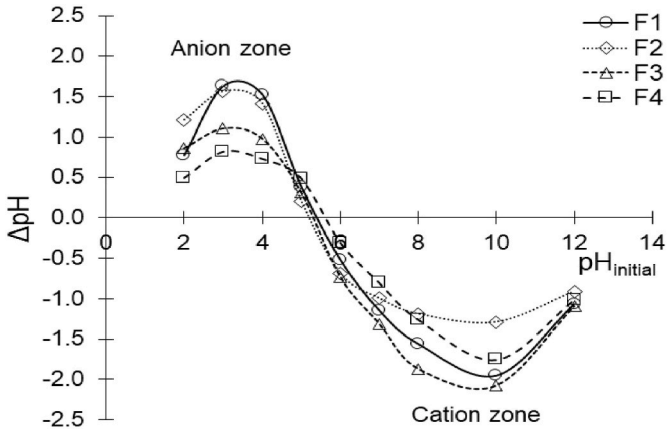

Fig. 3. Zero charge point curve for copolymers.

2.8. Multimetal adsorption evaluation

A multimetal solution of 5 ppm of Al, As, Cr, Hg, and Pb at pH 5 and 6 was prepared, 100 mg of the copolymer was added in 1000 mL and stirred at 100 rpm for 100 min; an aliquot was filtered at 0.45 μm [9]; and the reading of the residual concentration of metals was carried out through an ICP-OES 9820 Shimadzu (Kyoto, Japan), in axial mode, in quadruplicate, with rinsing between samples of 30 s at 60 rpm, and a gas flow of 10 L/min with plasma exposure of 30 s. Standard curves for each metal were previously prepared, with a regression coefficient $R^2 > 0.995$. The results of the adsorption were expressed as the percentage of removal.

2.9. Adsorption kinetics evaluation

The adsorption rate of the adsorbate on the adsorbent and the saturation or equilibrium time in which this process is achieved was determined by evaluating the adsorption kinetics [10,30].

Samples in multimetal solution were prepared considering the evaluation criteria of multimetal adsorption for each adsorption time (0, 20, 40, 60, 80, 100, and 120 min).

The experimental adsorption of metals in time (q_t) was determined through Equation (1) [11].

$$q_t = \frac{V(C_0 - C_t)}{m} \tag{1}$$

where C_t, is the metal concentration at time t (mg/L); C_o, is the initial concentration of the metal at t = 0.0 min (mg/L); V is the volume of the solution (L); m is the mass of the copolymer (mg).

The experimental data q_t obtained were fitted to pseudo-first order, pseudo-second order, Elovich, and intraparticle diffusion kinetic models [16,31,32].

2.9.1. Pseudo first order model

His model does not involve interaction or competition between ions for the active sites, the adsorption being maximum at the monolayer level, and it occurs with the same energy on the entire surface of the adsorbent.

$$ln(q_e - q_t) = ln(q_e) - k_1 t \tag{2}$$

where, q_e (mg/g) is the amount of metal adsorbed at equilibrium; q_t (mg/g) is the amount of metal adsorbed at time t; k_1 is the adsorption rate constant (min-1); t (min) is the contact time.

2.9.2. Pseudo second order model

The equation based on equilibrium adsorption was expressed through equation (3) [33,34].

$$\frac{t}{q_t} = \frac{1}{k_2 q_e^2} + \frac{t}{q_e} \tag{3}$$

where k2 (g/mg.min) is the kinetic constant of the pseudo second order model; t (min) is the contact time.

The initial rate of adsorption h (mg/g.min) is calculated through equation (4) [19].

Table 2
Particle size and ζ potential for copolymers.

F	Size (Peak 1, nm)					Size (Peak 2, nm)					ζ potential (mV)			
	$\bar{x}$	±S	CV	*	%	$\bar{x}$	±S	CV	*	%	$\bar{x}$	±S	CV	*
F1	370.07	16.79	4.54	a,b	87.44 ± 13.73	77.10	3.50	4.54	a	18.84 ± 11.84	−29.80	1.15	3.86	a
F2	338.80	4.91	1.45	b	89.83 ± 5.41	57.91	1.88	3.25	b	10.17 ± 5.41	−18.96	0.51	2.69	b
F3	422.83	15.32	3.62	c	100.00						−22.17	0.73	3.28	c
F4	381.03	11.15	2.93	a	98.22 ± 3.08	66.62	3.61	5.42	c	5.34 ± 0.00	−16.72	0.54	3.25	d

Where F, is formulation; $\bar{x}$, is the arithmetic mean; SD is the standard deviation; CV; variability coefficient.
* Evaluated through an ANOVA and Tukey's test at 5% significance, for $n = 3$.

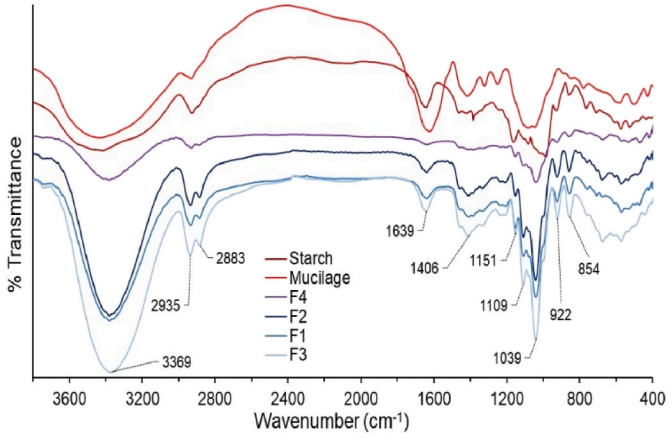

Fig. 4. FTIR spectra for starch, mucilage, and copolymers (F1, F2, F3, and F4).

$$h = k_2 q_e^2 \tag{4}$$

2.9.3. Elovich model

Elovich's exponential equation has general application in chemisorption phenomena, describing heterogeneous isotopic exchange reactions on the surface of the adsorbent as a function of the activation energy of the active sites. The constants of the equation allow for comparing the speed of adsorption in different materials, mainly clays [32].

$$q_t = \frac{1}{\beta}\ln(\alpha\beta) + \frac{1}{\beta}\ln(t) \tag{5}$$

where α is the initial rate of adsorption (mg/g.min); β is related to the extent of surface coverage and the activation energy for chemisorption (g/mg).

2.9.4. Intraparticle diffusion model

This model explains from the empirical point of view, the adsorption from a zone of high concentration to the solid phase through the diffusion/transport process, where the adsorption varies almost proportionally to $t^{1/2}$ instead of the time t [20,31].

$$q_t = k_{ip} t^{1/2} + C_i \tag{6}$$

where kip, intraparticle diffusion rate constant (mg/g.min1/2); Ci is the concentration at the level of the boundary layer i (mg/g).

If Ci is equal to zero, the only control step is intraparticle diffusion; if Ci ≠ 0, it indicates that the adsorption process is quite complex and involves more than one diffusive resistance.

2.10. Adsorption isotherms evaluation

Adsorption isotherms or equilibrium studies, are essential for designing adsorption systems, for example, treating heavy metals in wastewater. Their modeling is necessary to establish design parameters [21,33].

250 mL of a multimetal solution of As, Cd, Pb, and Zn of 10, 50, 100, 150, 200, and 250 ppm was prepared, added to 0.25 mg of the copolymer, stirred at 50 rpm for 90 min at 20 °C, adjusted the pH of the solution to 5 and 6 with 0.1 M NaOH and 0.1 M HNO3. An aliquot was filtered at 0.25 μm and taken to an ICP-OES 9820 Shimadzu (Kyoto, Japan).

The equilibrium adsorption capacity of heavy metals (q_e), was determined through Equation (7) [11].

$$q_e = \frac{V(C_0 - C_e)}{m} \tag{7}$$

where, C_e, is the concentration of adsorbate at equilibrium (mg/L); C_o, is the initial concentration of adsorbate (mg/L); V is the volume of the solution (L); m, is the mass of copolymer (adsorbent) (mg).

From the q_e and C_e data, the adsorption isotherm was constructed and fitted to the Langmuir, Freundlich, Redlich-Peterson, and Dubinin Radushkevich models.

2.10.1. Langmuir model

This model assumes equilibrium adsorption at the monolayer level of the adsorbent, which contains a surface with a finite number of identical sites [34,35] and is represented according to Equation (8)

$$q_e = \frac{q_m K_L C_e}{1 + K_L C_e} \tag{8}$$

where q_e is the equilibrium adsorption capacity (mg/g); k_L is Langmuir's constant (L/mg); C_e is the equilibrium concentration of the adsorbate (mg/L); qm is the adsorption capacity of the monolayer (mg/g).

The R_L separation factor, which measures the affinity between the adsorbate and adsorbent, makes it possible to predict the behavior of the adsorption system, if: $R_L > 1$ unfavorable, $R_L = 1$ Linear, $0 < R_L < 1$ favorable, $R_L = 0$ irreversible; and is calculated through Equation (9) [33,36].

$$R_L = \frac{1}{(1 + k_L C_0)} \tag{9}$$

2.10.2. Freundlich's model

The model assumes a homogeneous adsorption surface, with active sites of different adsorption energy (Equation (10)) [34,37,38].

$$q_e = k_f C_e^{1/n} \tag{10}$$

where k_f ($mg^{1-1/n}L^{1/n}$) and 1/n, are Freundlich's constants.

2.10.3. Redlich–peterson model

This three-parameter model arises from the combination of the Langmuir and Freundlich models and is used for homogeneous and

Table 3
Multimetal removal (%).

pH		Al				As				Cr				Hg				Pb				Total amount (mg/g)			
		$\bar{x}$	±SD	CV	*	$\bar{x}$	±SD	CV	*	$\bar{x}$	±SD	CV	*	$\bar{x}$	±SD	CV	*	$\bar{x}$	±SD	CV	*	$\bar{x}$	±SD	CV	*
6.00	F1	54.75	0.29	0.54	a	59.36	0.40	0.68	a	38.19	0.29	0.77	a	39.67	0.13	0.33	a	78.31	0.40	0.52	a	151.43	0.35	0.23	a
	F2	33.15	0.50	1.51	b	44.03	0.47	1.06	b	35.47	0.52	1.48	b	28.63	0.34	1.19	b	57.13	0.26	0.46	c	110.83	0.87	0.79	b
	F3	44.07	0.40	0.90	c	55.50	0.37	0.67	c	34.95	0.51	1.45	b	37.74	0.33	0.87	c	72.42	0.25	0.34	b	136.67	0.21	0.15	c
	F4	36.25	0.05	0.14	d	40.26	0.34	0.84	d	34.25	0.58	1.69	b	29.77	0.18	0.60	d	57.65	0.75	1.31	c	110.40	1.14	1.03	b
5.00	F1	50.88	0.59	1.16	a	57.43	0.24	0.42	a	36.66	0.40	1.09	a	38.05	0.42	1.10	a	73.80	0.24	0.32	a	143.54	0.42	0.29	a
	F2	31.64	0.20	0.64	c	41.85	0.46	1.09	b	33.74	0.47	1.40	b	25.14	0.55	2.19	c	56.14	0.18	0.33	b	105.40	0.36	0.34	b
	F3	42.33	0.09	0.22	b	52.06	0.24	0.45	c	31.41	0.45	1.44	c	34.68	0.84	2.42	b	71.03	0.39	0.55	c	129.50	0.10	0.08	c
	F4	32.86	0.80	2.43	c	39.51	0.14	0.35	d	30.84	0.44	1.43	c	25.32	0.32	1.26	c	54.29	0.14	0.25	d	102.20	0.53	0.52	d
p-value**		<0.05				<0.05				<0.05				<0.05				<0.05				<0.05			

Where $\bar{x}$, is the arithmetic mean; SD is the standard deviation; CV; the variability coefficient.
* Evaluated through an ANOVA and Tukey's test at 5% significance, for $n = 3$. **Evaluated through a bifactorial ANOVA at 5% significance.

heterogeneous sorption systems in the liquid phase of heavy metals and is represented through Equation (11) [39–41].

$$q_e = \frac{K_R C_e}{1 + a_R C_e^{\beta}} \tag{11}$$

where K_R (L/g), a_R $(L/mg)^{1/\beta}$, and β are the isotherm constants.

The value of β allows for knowing the mechanism of adsorption. If it is between 0 and 1, it indicates heterogeneous and favorable adsorption; $\beta = 1$, physisorption is the main mechanism of adsorption, and if $\beta = 0$ it shows that the adsorption isotherm is linear [39,42].

2.10.4. Dubinin–raduskevich model

The model allows to determine the free energy of adsorption of physical or chemical process, whose expression is shown in Equation (12) [38,40,43].

$$q_e = q_D \exp\left(-B\varepsilon^2\right) \tag{12}$$

where q_e is the equilibrium adsorption capacity (mg/g); q_D is the theoretical saturation capacity (mg/g); B is the constant related to the average free energy of adsorption (mol2/kJ2); and ε is the Polanyi Potential, which is related to the adsorption equilibrium. Likewise, it allows calculating the average adsorption energy (E) per sorbate molecule as if it were an infinite surface of the adsorbent (Equation (13)).

$$E = 1 \Big/ (2B)^{1/2} \tag{13}$$

If $E < 8$ kJ/mol, the adsorption is physical, and if $E > 8$ kJ/mol, the adsorption is of a chemical nature, while intermediate values of $8 = E \leq 16$ kJ/mol mean ion exchange [38,44].

2.11. Experimental data fit

The parameters of the kinetic and isotherm models were calculated through non-linear regression, fitting to the experimental data, considering the minimum difference of squares as a convergence criterion, evaluated through the Quasi-Newton (QN), Simplex/Quasi-Newton (SQN) and Rosenbrock/Quasi-Newton (RQN) methods [45,46]. Similarly, error function statistical tools were used to discriminate the models used numerically. The adjustment coefficient R^2 was calculated, which measures the variability of the dependent variable of the adjusted model. The average relative error (*ARE*) that allows minimizing the distribution of the fractional error; and the Chi-square test (X^2), which is based on the minimum difference of squares, were determined by Equations (14) and (15), respectively [22,47–49].

$$ARE = \frac{100}{N} \sum_{i=1}^{N} \left| \frac{q_{adj} - q_{exp}}{q_{exp}} \right|_i \tag{14}$$

$$X^2 = \sum_{i=1}^{N} \left[\frac{\left(q_{exp} - q_{adj}\right)^2}{q_{adj}} \right]_i \tag{15}$$

where q_{adj} is the adsorption capacity reported by the model; $q_{\exp}$ is the experimental adsorption capacity; N, is the data number.

Values of R^2 close to unity indicate a good fit of the model, while *ARE* and X^2 should be as low as possible [22,33,50].

The dispersion of the residuals was also evaluated, whose criteria were: random (RD), slightly random (SR), and trending (T). The models with the best fit were randomly distributed.

The analyzes were performed with a significance level of 5%, using Excel spreadsheets, the Solver utilitarian, and Statistica V12 software.

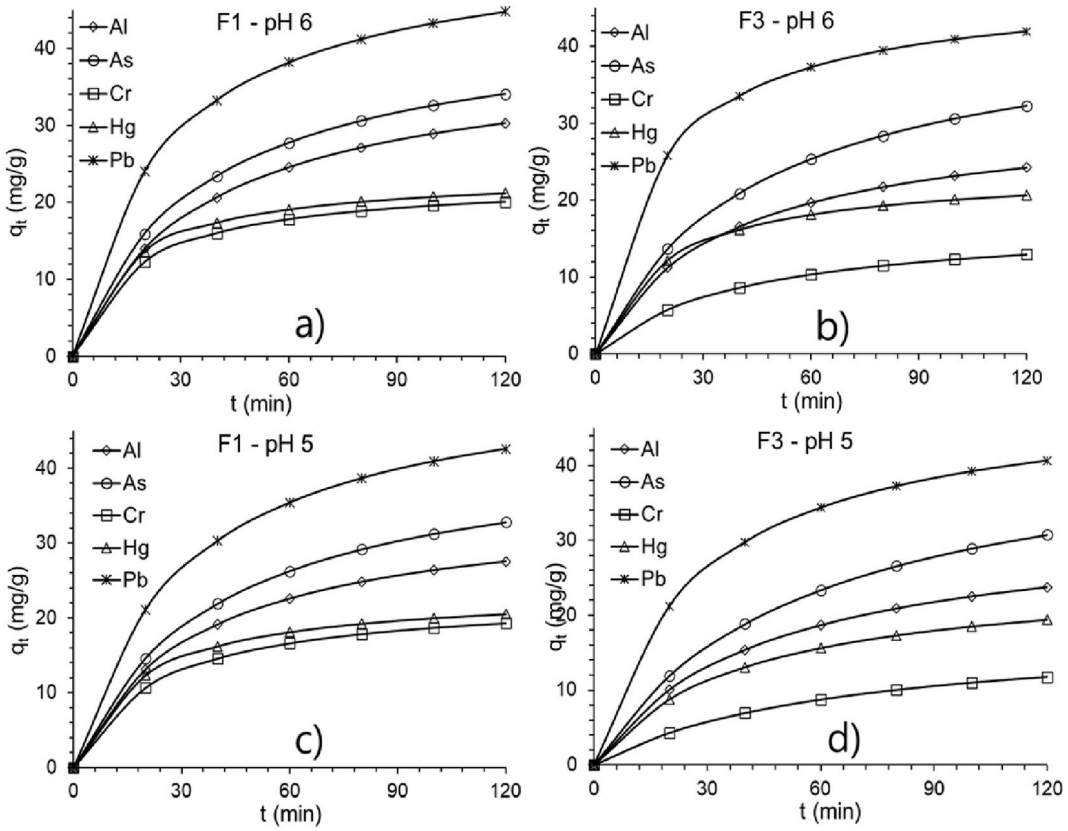

Fig. 5. Curves fitted to the pseudo second order kinetic model, a) copolymer F1 at pH 6; b) copolymer F3 at pH 6; c) copolymer F1 at pH 5; d) copolymer F3 at pH 5.

3. Results and discussion

3.1. Solubility of copolymers

It was observed that the solubility of the F1 copolymer was higher, followed by F3 (Fig. 2); both formulations have a higher content of nopal mucilage (MS). Aqueous media at neutral and acidic pH increase solubility, showing no significant difference. The effects on solubility are generally significant (p-value <0.05) for SS, MS, and solvent pH.

Adding nopal mucilage in copolymers allows for a considerable increase in solubility [51,52] due to the presence of sugars and hydrophilic proteins [53,54]. Although in general, the solubility of the copolymers does not reach 100% or close values, which would be considered a disadvantage; however, the use of fully biodegradable materials makes it potential for use, compared to other materials of inorganic or organic/inorganic origin [55,56].

3.2. Zero point charge, ζ potential, and particle size

The adsorbent's zero charge point or zero potential (pHzpc) allows knowing the surface charge of the adsorbent within a pH range sensitive to ionic attractions in the solvent medium [57,58]. Thus, if the pH < pHzpc (pH of the solution), the surface of the adsorbent attracts anions from the solution since the surface of the adsorbent is positively charged [20,58,59].

It was observed that the pHzpc of the copolymers is around 5.5 (Fig. 3) and that, for higher values, the surface of the copolymer is negatively charged, so it would have the availability to attract cations. This would be justified due to the arrangement of groups with a partial negative charge, such as hydroxyl, carbonyl, and carboxyl mainly, on the surface of the studied material.

The ζ potential allows knowing the stability of a material in an aqueous solution through the determination of the surface charge. The absolute value greater than 40 mV indicates high stability, between 20 and 40 mV medium stability, and less than 20 mV allows easy agglomeration and sedimentation [10,60,61], although it could be related to the particle size [23].

Values between 16.72 and 29.80 mV were reported (Table 2), indicating medium stability, which is advantageous for a material such as the one studied since it would not allow much time in suspension and, at the same time, it would not sediment easily, thus capturing the most significant amount of dissolved metals. This suggests that the surface of the copolymer would be negatively charged, which is justified, since its constituents, such as starch and nopal mucilage, present functional groups such as hydroxyl, carbonyl, carboxyl, amino, phosphoryl, sulfhydryl, among others with negative sides [23,60,62].

On the other hand, it was observed that the particle size is distributed in two groups, the first between 338.80 and 422.83 nm (Table 2), while the second group between 57.91 and 77.10 nm, being at the nanometric level.

3.3. FTIR spectral analysis of the copolymers

The ability of the copolymer to adsorb cations can be established by the presence and intensity (an indirect measure of the amount) of negatively charged functional groups.

The peak around 3369 cm^{-1} is attributed to the vibration of the stretching of the hydrogen bond of the OH and NH groups coming from the carbohydrates and primary amines of the starch and mucilage, which have an affinity for metal adsorption [60,63], observing greater intensity in the order F3>F1>F2»F4 (Fig. 4). The spectra near 2935 and 2883 cm^{-1} belong to the asymmetric and symmetric vibration of CH of the alkyl groups of the polymeric chains of carbohydrates and proteins mainly [64]. Also, around 1639 cm^{-1}, the vibration of COOH and NH stretching is observed [65], with greater intensity for F1 and F3, whose formulation presents greater content of nopal mucilage; these groups

Table 4
Adjustment coefficients for kinetic models.

Metal ion	Model	F1 - pH 6					F3 - pH 6					F1 - pH 5					F3 - pH 5				
		R^2	X^2	ARE	EM	Res	R^2	X^2	ARE	EM	Res	R^2	X^2	ARE	EM	Res	R^2	X^2	ARE	EM	Res
Al	PSFO	0.993	0.293	3.939	QN	R	0.986	0.430	5.229	QN	R	0.980	0.669	6.245	QN	R	0.995	0.154	3.327	QN	R
	PSSO	0.997	0.113	2.607	QN	R	0.991	0.230	4.221	QN	R	0.988	0.353	4.751	RQN	R	0.993	0.168	3.299	RQN	R
	Elovich	0.998	0.071	1.999	SQN	R	0.993	0.155	3.411	RQN	R	0.992	0.214	3.856	SQN	R	0.990	0.230	4.040	QN	R
	IPD	0.987	0.309	3.658	RQN	R	0.983	0.321	4.212	SQN	SR	0.982	0.444	4.981	QN	R	0.981	0.404	4.548	QN	SR
As	PSFO	0.990	0.434	4.490	QN	R	0.992	0.325	4.174	QN	R	0.990	0.431	4.333	QN	R	0.990	0.332	4.181	QN	R
	PSSO	0.993	0.230	3.685	QN	R	0.990	0.326	4.144	QN	R	0.994	0.202	3.459	RQN	R	0.987	0.430	4.812	QN	R
	Elovich	0.994	0.182	2.874	SQN	R	0.988	0.394	4.346	RQN	R	0.996	0.122	2.690	QN	R	0.983	0.553	5.788	RQN	R
	IPD	0.981	0.479	4.567	QN	R	0.979	0.612	4.751	SQN	R	0.989	0.281	3.571	QN	R	0.974	0.835	7.249	QN	SR
Cr	PSFO	0.967	0.679	7.434	QN	SR	0.999	16.098	34.038	QN	R	0.960	0.815	8.656	QN	R	0.993	13.352	32.584	QN	R
	PSSO	0.985	0.299	5.001	RQN	SR	0.998	15.998	33.751	QN	R	0.978	0.413	6.422	RQN	R	0.991	13.413	32.336	RQN	R
	Elovich	0.994	0.124	3.149	SQN	R	0.995	16.086	33.621	SQN	R	0.988	0.216	4.579	SQN	R	0.988	13.556	32.221	QN	R
	IPD	0.943	1.044	7.179	RQN	T	0.982	16.963	34.413	QN	R	0.962	0.707	6.388	QN	SR	0.978	13.792	31.474	QN	R
Hg	PSFO	0.980	0.399	5.620	QN	SR	0.995	0.100	2.742	QN	R	0.984	0.343	5.071	QN	R	0.999	0.020	1.215	QN	R
	PSSO	0.994	0.127	3.144	QN	R	1.000	0.007	0.796	QN	R	0.995	0.105	2.896	QN	R	0.996	0.096	2.752	RQN	R
	Elovich	0.999	0.030	1.429	RQN	R	0.998	0.035	1.603	QN	SR	0.998	0.030	1.672	QN	R	0.990	0.212	4.338	QN	R
	IPD	0.925	1.285	8.218	RQN	T	0.941	0.887	8.361	SQN	T	0.944	0.916	7.714	QN	T	0.973	0.467	6.448	QN	T
Pb	PSFO	0.993	0.332	3.702	QN	SR	0.996	0.158	2.519	QN	R	0.992	0.433	4.148	QN	R	0.993	0.331	3.865	QN	R
	PSSO	0.998	0.066	1.412	QN	R	1.000	0.007	0.443	QN	T	0.997	0.127	2.254	RQN	R	0.998	0.062	1.647	SQN	R
	Elovich	0.999	0.061	1.634	SQN	SR	0.998	0.093	1.923	QN	R	0.998	0.058	1.349	QN	R	0.999	0.031	1.133	QN	SR
	IPD	0.966	1.155	6.350	SQN	SR	0.928	2.195	8.921	SQN	T	0.979	0.661	4.891	QN	T	0.972	0.871	5.692	QN	T

have an affinity to bind cations. The peaks around 1406 cm^{-1} are attributed to the C═O groups of amides I, II, and III [66]. At 1406 cm^{-1}, the CN and NH stretching vibration of amides II and CO [67] from mucilage are manifested. Spectra between 1151 and 1039 cm^{-1} present high intensity, and are attributed to CH and COC bending vibrations of polysaccharides and esters [67]. Likewise, the peaks between 922 and 854 cm^{-1} are related to the CO bending vibrations of the polysaccharides and esters [23,66,68].

Low-intensity spectra ranging from 1406 to 854 cm^{-1} represent a specific region of polysaccharides and proteins [23,29,67,69,70]. In general, the peaks in the interval of the spectra shown in Fig. 4 are characteristic of hydroxyl, carbonyl, carboxyl, amino, and amide groups, observing in most cases high intensity mainly for copolymers F1 and F3, which gives it a high affinity for metal adsorption [10,18,33,60,71].

3.4. Multimetal adsorption

The copolymers offered higher adsorption affinity for Pb, reaching up to 78.31% removal at pH 6.0 for the F1 formulation and 73.80% at pH 5.0 (Table 3). Likewise, adsorption of 59.36% and 57.43% was reported for As, Al 54.75 and 50.88%, Hg 39.67 and 38.05%, and Cr 38.19 and 36.66% at pH 6 and 5, respectively (Table 3).

The F1 copolymer reported a higher percentage of adsorption, followed by F3; this would be due to the higher mucilage content they present, which is mainly constituted by polysaccharides and water-soluble proteins with ionizable hydroxyl, carboxyl, and carbonyl functional groups [26,72,73], likewise due to the availability of the groups of starch [24,25].

On the other hand, the pH reported a significant effect (p-value <0.05), with greater adsorption at pH 6 for all metals. This would be associated with the solubility of metals since they precipitate at pH values for $As^{3+}>11$, $Pb^{2+}>7$, $Al^{3+}>4$, $Hg^{2+}>4$, and $Cr^{3+}>5$; as well as the availability of negatively charged functional groups such as carbonyl, carboxyl, and hydroxyl, located on the surface, pores, and interstices of the material, checking the pHzpc value found.

The total amount of metal adsorption was around 151.43 mg/g of copolymer at pH 6 and 143.54 mg/g at pH 5. These values agree with other studies [24,26,27,74]. However, it has been observed that synthesized materials of mineral or inorganic origin, presented higher removal of metals in unimetal systems reporting values of up to 3000 mg of Pb/g and 500 mg Cr/g [75,76].

3.5. Adsorption kinetics

The adsorption process contemplates the mass transfer and chemical reactions between the adsorbate and adsorbent. These are described through three stages, i) the adhesion of the sorbate to the external surface of the adsorbent, ii) the internal diffusion of the adsorbate into the active sites, and iii) the sorption itself onto the adsorbent. Three models based on reactions (PSFO, PSSO, and Elovich) and a diffusional model (ID) have been studied. These models allow knowing the rate or velocity of adsorption and the parameters of each model under certain assumptions and limitations, whose data are essential to design and model adsorption processes [10,17,39,40,77].

It was observed that the adsorption developed rapidly during the first 40 min (Fig. 5), during which time the active sites on the copolymer surface would be occupied due to the complexation of the –NH, –OH, C═O, COO groups with the metal ions, what supposes adsorption by chemisorption, allowing the formation of coordination chemical bonds; while at higher times, the adsorption occurs slowly, which could mean adsorption by diffusion; however, these processes are also regulated by the zeta potential and particle size [26,62,72,78,79].

The PSFO model was estimated through the QN method, reporting values of $R^2 > 0.960$, $X^2 > 0.020$, and $ARE > 1.215$, with a random distribution of residuals (Table 4). It was observed that the amount of

Table 5
Parameters of kinetic models.

Treatment	Metal ion	PSFO		PSSO			Elovich		ID	
		q_e	K_1	q_e	K_2 (x10^{-3})	h	α	β	k_{ip}	C_i
F1-pH 6	Al	30.878 *	0.028 *	39.522 *	0.690 *	1.078	1.594 *	0.097 *	2.825 *	1.239 **
	As	34.687 *	0.028 *	44.150 *	0.638 *	1.243	1.876 *	0.088 *	3.174 *	1.520 **
	Cr	19.674 *	0.044 *	23.030 *	2.458 *	1.304	3.537 **	0.222 *	1.838 *	2.226 **
	Hg	20.682 *	0.049 *	23.857 *	2.794 *	1.590	5.400 *	0.232 *	1.924 *	2.708 **
	Pb	44.336 *	0.036 *	54.117 *	0.736 *	2.156	4.031 *	0.081 *	4.133 *	3.500 **
F3-pH 6	Al	24.782 *	0.028 *	31.598 *	0.869 *	0.867	1.301 *	0.122 *	2.259 *	1.036 **
	As	33.507 *	0.025 *	44.344 *	0.501 **	0.986	1.315 *	0.080 *	3.026 *	0.638 **
	Cr	13.218 *	0.027 *	17.227 *	1.452 *	0.431	0.596 *	0.212 *	1.212 *	0.380 **
	Hg	20.238 *	0.042 *	23.962 *	2.157 *	1.238	2.994 *	0.205 *	1.883 *	2.177 **
	Pb	41.027 *	0.046 *	47.990 *	1.210 *	2.786	7.787 **	0.108 *	3.809 *	4.926 **
F1-pH 5	Al	27.990 *	0.029 *	35.312 *	0.836 *	1.042	1.630 *	0.112 *	2.563 *	1.372 **
	As	33.802 *	0.026 *	43.664 *	0.576 *	1.098	1.572 *	0.085 *	3.064 *	1.108 **
	Cr	19.144 *	0.036 *	23.045 *	1.859 **	0.987	2.015 **	0.198 *	1.783 *	1.628 **
	Hg	20.141 *	0.043 *	23.697 *	2.283 **	1.282	3.295 *	0.212 *	1.876 *	2.231 **
	Pb	42.844 *	0.031 *	53.495 *	0.611 *	1.749	2.867 *	0.076 *	3.959 *	2.512 **
F3-pH 5	Al	24.680 *	0.025 *	32.646 *	0.682 *	0.727	0.965 *	0.108 *	2.232 *	0.453 **
	As	32.801 *	0.021 *	45.022 *	0.399 **	0.810	0.992 *	0.073 *	2.907 *	−0.095 **
	Cr	12.829 *	0.020 *	18.029 *	0.869 *	0.282	0.331 *	0.173 *	1.118 *	−0.222 **
	Hg	19.734 *	0.028 *	25.620 *	1.015 *	0.666	0.930 *	0.144 *	1.819 *	0.629 **
	Pb	40.462 *	0.034 *	49.772 *	0.748 *	1.854	3.303 *	0.086 *	3.764 *	2.910 **

Where PFO, pseudo first order model; PSO, pseudo-second-order model; ID, Intraparticle Diffusion model.
*Significant; **Not significant, evaluated at 5% significance.

Table 6
Adjustment coefficients for adsorption isotherms.

Metal ion	Model	pH 6					pH 5				
		R^2	X^2	ARE	EM	Res	R^2	X^2	ARE	EM	Res
AS	Langmuir	0.953	92.779	17.022	QN	T	0.983	11.744	8.986	QN	R
	Freundlich	0.974	36.297	11.867	QN	T	0.990	13.099	11.496	QN	R
	Redlich-Peterson	0.975	39.941	14.572	RQN	T	0.994	4.403	6.219	QN	R
	Dubinin Radushkevich	0.766	212.451	36.653	QN	T	0.881	82.818	27.199	QN	T
Pb	Langmuir	0.948	446.448	24.600	QN	T	0.992	6.452	13.740	QN	R
	Freundlich	0.994	23.467	10.770	RQN	R	0.980	50.995	18.710	QN	R
	Redlich-Peterson	0.979	10.954	3.964	RQN	R	0.996	36.470	8.928	QN	R
	Dubinin Radushkevich	0.815	212.451	32.356	QN	T	0.905	82.818	28.318	QN	T
Al	Langmuir	0.986	14.175	9.177	QN	SR	0.982	28.244	12.459	QN	SR
	Freundlich	0.986	12.598	9.884	RQN	SR	0.995	3.513	5.568	RQN	R
	Redlich-Peterson	0.989	16.864	11.482	RQN	T	0.966	2.590	4.025	QN	SR
	Dubinin Radushkevich	0.920	28.809	25.806	QN	T	0.860	46.315	29.901	QN	T
Hg	Langmuir	0.867	114.278	24.760	QN	SR	0.951	25.939	14.033	QN	SR
	Freundlich	0.905	38.031	15.109	QN	T	0.978	7.187	8.346	RQN	R
	Redlich-Peterson	0.913	38.459	14.852	QN	T	0.978	6.941	7.997	QN	SR
	Dubinin Radushkevich	0.682	98.784	36.061	QN	T	0.830	35.355	28.694	QN	T
Cr	Langmuir	0.899	45.225	18.956	QN	SR	0.863	19.941	11.576	QN	SR
	Freundlich	0.944	13.954	9.269	QN	T	0.887	23.826	18.071	QN	R
	Redlich-Peterson	0.945	14.964	10.585	QN	T	0.893	18.821	14.245	QN	SR
	Dubinin Radushkevich	0.756	46.551	30.558	QN	T	0.751	27.801	27.814	QN	SR

Where R^2, adjustment coefficient; X^2, Chi-Square; ARE, average relative error; EM, estimation method; Res, residuals trend; R, random; SR, slightly random; T, trending; QN, Quasi-Newton method; RQN, Rosenbrock, and Quasi-Newton method.

metal absorbed at equilibrium (q_e) for the PSFO model was between 13.218 and 44.336 mg/g at pH 6 and from 12.829 to 42.844 mg/g at pH 5 in the order Pb > As > Al > Hg > Cr for F1 and F3 copolymers (Table 5). On the other hand, the adsorption rate K_1 was higher for Hg 0.049 min^{-1} in F1, and in F3, it was higher for Pb 0.046 min^{-1} at pH 6, respectively; the same behavior is reported at pH 5, although with slightly lower values.

The PSSO model was estimated through the QN and RQN method, reporting $R^2 > 0.978$, $X^2 > 0.007$, and $ARE > 0.443$, and random residual distribution (Table 4). It was observed that q_e values ranged from 17.227 to 54.117 mg/g for F1 and F3 copolymers in the order Pb > As > Al > Hg > Cr, while K_2 ranged from 0.399×10^{-3} to 2.794×10^{-3} g/mg. min presenting lower values for As and Pb. On the other hand, the initial adsorption velocity, h, is higher for Pb, followed by Hg and As, with similar values for Cr and Al for the F1 and F3 copolymers at the studied pH, high values suggest higher adsorption capacity in materials of organic and inorganic nature [20,25,80].

Where PFO, pseudo first order model; PSO, pseudo-second-order model; ID, Intraparticle Diffusion model; R^2, adjustment coefficient; X^2, Chi-Square; ARE, average relative error; EM, estimation method; Res, residuals trend; R, random; SR, slightly random; T, Trending; QN, Quasi-Newton method; SQN, Simplex, andQuasi-Newton method; RQN, Rosenbrock, and Quasi-Newton method.

To estimate the Elovich model, the QN, SQN, and RQN methods were applied, and it was observed that the initial adsorption velocity α was between 0.331 and 7.787 mg/g. min being higher for Pb and Hg in F1 and F3. The constant β is related to the extent of surface coverage and the activation energy for chemisorption, and it was found to be between 0.073 and 0.232 g/mg being lower for Pb and As (Table 5). These constants would be indirectly involved with the reaction rate during chemisorption, thus the decrease β and increase α improve the velocity of adsorption [32], which is verified with the order of adsorption Pb >

Table 7
Parameters of the adsorption isotherm models.

pH	Metal ion	Langmuir		Freundlich			Redlich-Peterson			Dubinin Radushkevich	
		q_{max}	K_L	K_F	n	1/n	K_R	a_R	β	q_D	B
6	As	1578.773	0.006	28.671	1.559	0.642	−19.856	−1.371	0.264	631.560	8.91×10^{-5}
		**	**	**	*		undf	undf	undf	*	**
	Pb	1661.954	0.054	252.341	2.585	0.387	−94.096	−0.959	0.435	1191.309	0.29×10^{-5}
		*	**	**	*		undf	undf	undf	*	**
	Al	831.731	0.011	34.448	1.854	0.539	−48.854	−1.951	0.411	523.550	17.25×10^{-5}
		*	*	**	*		undf	undf	undf	*	**
	Hg	952.670	0.004	14.067	1.571	0.637	−1.968	−0.940	0.137	348.544	16.94×10^{-5}
		**	**	**	**		undf	undf	undf	*	**
	Cr	466.915	0.011	22.471	1.975	0.506	−29.903	−1.813	0.445	294.085	14.99×10^{-5}
		*	**	**	*		undf	undf	undf	*	**
5	As	694.785	0.014	39.829	2.028	0.493	24.718	0.261	0.653	466.622	11.37×10^{-5}
		*	**	*	*		undf	undf	undf	*	**
	Pb	1422.853	0.057	234.239	2.766	0.362	133.021	0.210	0.837	1108.314	0.99×10^{-5}
		*	*	*	*		undf	undf	undf	*	**
	Al	742.084	0.009	28.088	1.840	0.543	53.253	1.455	0.498	435.935	16.50×10^{-5}
		*	**	*	*		undf	undf	undf	*	**
	Hg	519.980	0.010	22.916	1.920	0.521	165.914	6.796	0.489	326.153	17.09×10^{-5}
		*	**	*	*		undf	undf	undf	*	**
	Cr	270.130	0.028	29.740	2.533	0.395	20.298	0.361	0.717	219.333	8.80×10^{-5}
		*	**	**	**		undf	undf	undf	*	**

Where undf, undefined.
*Significant at 5%.
**Not significant at 5%.

Table 8
RL values for adsorption evaluated through the Langmuir model.

pH	Initial concentration, C_0 (mg/L)	As		Pb		Al		Hg		Cr	
		Final concentration, C_f (mg/L)	R_L	Final concentration, C_f (mg/L)	R_L	Final concentration, C_f (mg/L)	R_L	Final concentration, C_f (mg/L)	R_L	Final concentration, C_f (mg/L)	R_L
6	10.0	4.196	0.948	0.230	0.648	4.380	0.901	5.190	0.963	5.19	0.96
	50.0	22.007	0.783	3.624	0.269	29.860	0.646	32.633	0.840	34.02	0.84
	100.0	64.372	0.644	19.840	0.155	63.369	0.477	78.658	0.724	79.96	0.72
	150.0	97.173	0.546	45.078	0.109	108.257	0.378	123.560	0.637	125.75	0.64
	200.0	133.417	0.475	67.615	0.084	149.425	0.313	168.117	0.568	172.74	0.57
	250.0	170.575	0.420	100.201	0.069	191.426	0.267	202.413	0.513	212.48	0.51
5	10.0	4.533	0.875	0.440	0.638	4.523	0.914	5.327	0.905	5.947	0.905
	50.0	27.467	0.582	6.837	0.261	30.567	0.681	33.980	0.656	34.733	0.656
	100.0	68.033	0.411	22.350	0.150	72.750	0.516	77.050	0.488	82.433	0.488
	150.0	108.816	0.317	49.807	0.105	112.647	0.416	124.297	0.389	132.087	0.389
	200.0	153.756	0.259	80.603	0.081	155.927	0.348	168.107	0.323	179.317	0.323
	250.0	196.010	0.218	123.940	0.066	200.353	0.299	210.837	0.276	222.083	0.276

Table 9
Values of average adsorption energy (kJ/mol).

pH	As	Pb	Al	Hg	Cr
6	0.08	0.41	0.05	0.05	0.06
5	0.07	0.23	0.06	0.05	0.08

As > Al > Hg > Cr; these values are consistent for multimetal adsorption systems [13,17].

The intraparticle diffusion model, estimated through the QN, SQN, and RQN methods, showed that the intraparticle diffusion rate constant, kip, is between 1.118 and 4.133 mg/g. $min^{1/2}$ and follows the order Pb > As > Al > Hg > Cr, high values are indicative that the diffusion/transport process manifests rapidly in the pores of the copolymer surface, having a higher affinity for Pb and As [10,80]. Likewise, values of C > 0 (concentration at the level of the boundary layer i) indicate that the adsorption process would be not only subject to intraporous diffusion and chemisorption but also to other complex mechanisms, which would mean that there is more than one diffuse resistance such as pore size in the copolymer [12,20,25,26,31].

The reported values of R^2, X^2, *ARE*, and residual analysis (Table 4)

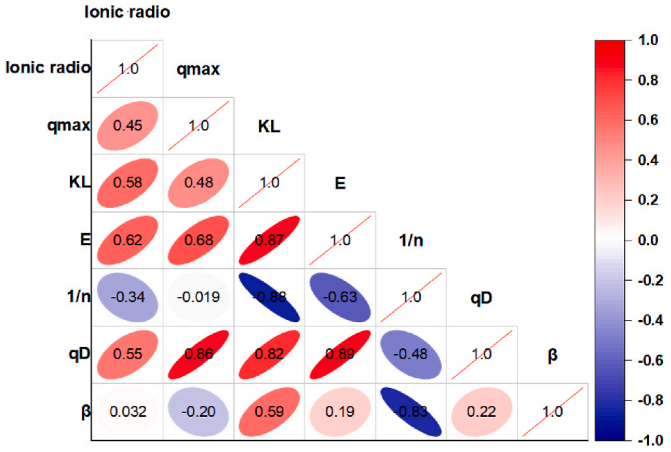

Fig. 6. Parameter correlation of isotherm models.

for the PSFO, PSSO, and Elovich models suggest that adsorption is produced by the chemisorption mechanism, which implies the establishment of bonds between the metal ions and the functional groups of the copolymers, in the same way, it would be affirmed that the adsorption is also manifested by diffusional means evaluated through the ID model. These results are similar to those reported for materials of organic and biological origin [20,24,41,81–83].

3.6. Adsorption isotherms

Adsorption isotherms reveal the maximum adsorption capacity of the metal ions in the copolymer, how they migrate to the active sites on the surface and inside the copolymer, the amount of energy involved, and the migration rate [20,24].

The Langmuir model was estimated through the QN method and reported R^2>0.863. However, for the adsorption of As, Pb, and Al, it was higher, showing the dispersion of residuals between random (R) and trending (T) (Table 6). The values of the maximum adsorption at the monolayer level (q_m) in the F1 copolymer were found between 466.915 and 16661.954 at pH 6 and between 270.130 and 1422.853 at pH 5, showing selectivity in the order Pb > As > Hg > Al > Cr at pH 6, and Pb > Al > As > Hg > Cr at pH 5 (Table 7).

The K_L parameter is related to the binding energy in the active sites. Higher values were observed for Pb at pH 5 and 6 (Table 7), which would indicate that the copolymer has a greater affinity for this ion, and would be favored by the atomic radius of Pb^{2+}, generating antagonism with the other ions [36,84], despite the adsorption process of the multimetal/copolymer solution system, is favorable for all metal ions (presence of chelating effect), since it reported values of the factor of separation R_L < 1.0 (Table 8), these results are usual for materials of biological origin [10,25,33,77,83].

The Freundlich model reported R^2 > 0.887, ARE <18.710, dispersion of residuals between random (R) and slightly random (SR) (Table 6), reporting values of the relative adsorption capacity K_F in the order Pb » Al > As > Cr > Hg at pH 6 and Pb » As > Cr > Al > Hg at pH 5 (Table 7), the fact that K_F is markedly different for metal ions is due to the hydration radius, pH of the medium, and the particle size of the copolymer [20,85–88], this is typical behavior for these materials [20,24,43].

The results report high saturation of the copolymer, mainly for Pb, since $1/n$ < 1.0, and indicate that it presents a heterogeneous surface structure with exponential distribution of the active sites since 0.0 < $1/n$ < 1.0 [12,16,50], which would indicate that they present favorable adsorption for all metal ions, because 1 < n < 10 [36,80,85,89].

Regarding the Redlich-Peterson model, it presents fit with R^2>893, X^2<39.941, ARE<14.852, and distribution of residuals between random and trending (Table 6); this model fits similarly to the Langmuir and Freundlich models as evidenced in other studies [40,90]. The β values found are less than 1.00, suggesting that adsorption is heterogeneous and favorable [39,40,42,47].

The Dubinin Radushkevic (D-R) model is generally applied to adsorption processes that occur on homogeneous and heterogeneous surfaces, with a pore-filling mechanism [91], reporting entirely tendentious residual distribution and R^2 values around 0.70 (Table 6). It was observed that the average adsorption energy was in the range of 0.054–0.075 kJ/mol at pH 6 and from 0.05 to 0.23 kJ/mol at pH 5 (Table 9), being higher for Pb, which suggests a predominance of physical adsorption mechanisms, which generally occurs in materials of biological origin [38,44,80,82,88,92,93], in the same way, it was observed that the theoretical saturation capacity reported values up to 1191.309 mg/g at pH 6 and 1108.314 mg/g at pH 5 for the Pb (Table 7).

The selectivity of metal ions is related to the atomic radius [36,84]. It was observed that they present a high positive correlation with q_{max} (adsorption capacity in the monolayer), K_L, E, and q_D (Fig. 6). In the same way, it was observed that K_L (parameter related to the binding energy in the active sites) shows an inverse relationship with $1/n$ (indirect measurement of the availability of active adsorption sites in the copolymer) and a direct relationship with the theoretical saturation capacity (q_D).

4. Conclusions

The copolymers formulated with native potato starch and nopal mucilage showed high solubility for nopal mucilage levels of 5% w/w, with a particle size in aqueous solution less than 422.83 nm, zero charge point around pH 5.5 and ζ potential between −16.72 and −29.80 mV, indicating medium stability in aqueous medium and high affinity for metal cations, confirmed through FTIR analysis, presenting anionic functional groups with chelating capacity. Multimetal adsorption in solution was reported, between 102.20 and 151.43 mg/g, with affinity in the order Pb > As > Al > Hg > Cr, being higher at pH 6 (p-value <0.05). The kinetic data were adequately fitted to the PSFO, PSSO, and Elovich models with R^2>0.994, X^2< 16.098, ARE<34.038, and dispersion of random residuals; the parameters of the models indicate that chemisorption processes would dominate the system. The adsorption isotherms were significantly adjusted to the Langmuir, Freundlich, and Redlich-Peterson models with R^2>0.863, whose parameters are closely related to the ionic radius of the metals, suggesting favorable adsorption and the heterogeneous surface of the copolymer. The mean adsorption energy values were found to be between 0.05 and 0.23 kJ/mol. Using native potato starch and nopal mucilage allows the formulation of copolymeric materials with a high potential for multimetal adsorption in aqueous systems.

Credit author statement

David Choque-Quispe: Conceptualization, Methodology, Formal analysis, Investigation, Writing - Original Draft, Writing - Review & Editing, Supervision; **Carlos A. Ligarda-Samanez:** Methodology, Validation, Writing - Original Draft, Writing - Review & Editing; **Yudith Choque-Quispe:** Formal analysis, Data Curation, Software; **Aydeé M. Solano-Reynoso:** Formal analysis, Project administration; **Betsy S. Ramos-Pacheco:** Methodology, Formal analysis, Writing - Review & Editing; **Miluska M. Zamalloa-Puma:** Formal analysis, Visualization; **Genaro Julio Álvarez-López:** Validation, Visualization; **Alan Zamalloa-Puma:** Software; Formal analysis**; Katya Choque-Quispe:** Validation, Data Curation; **Humberto Alzamora-Flores:** Formal análisis, Writing - Original Draft.

Funding

This research was funded by Vicepresidencia de Investigación de la Universidad Nacional José María Arguedas, Andahuaylas, Apurímac, Perú.

Declaration of competing interest

The authors declare that they have no known competing financial interests or personal relationships that could have appeared to influence the work reported in this paper.

Data availability

Data will be made available on request.

Acknowledgments

The authors would like to thank the Vice Presidency of Research of the Universidad Nacional José María Arguedas, for the financing and use of the water analysis and control research laboratory and Food Nanotechnology Research Laboratory. In the same way to the Dirección de Innovación y Transferencia Tecnológica - UNAJMA , Instituto de Investigación – UNAJMA, as a National Support Institution, and to the

Dirección de Gestión de la Innovación Agraria - INIA, Perú (R. D. N° 007-2022-INIA-DGIA, and the Contract for access to Genetic Resources No. 002-2022-MIDAGRI-INIA/DGIA).

References

[1] K.M. Mohiuddin, H.M. Zakir, K. Otomo, S. Sharmin, N. Shikazono, Geochemical distribution of trace metal pollutants in water and sediments of downstream of an urban river, Int. J. Environ. Sci. Technol. 7 (2010) 17–28, https://doi.org/10.1007/BF03326113.

[2] D. Choque-Quispe, S. Froehner, C.A. Ligarda-Samanez, B.S. Ramos-Pacheco, D. E. Peralta-Guevara, H. Palomino-Rincón, Y. Choque-Quispe, A.M. Solano-Reynoso, G.I. Barboza-Palomino, F. Taipe-Pardo, et al., Insights from Water Quality of High Andean Springs for Human Consumption in Peru 13 (2021) 2650, https://doi.org/10.3390/w13192650.

[3] D. Choque-Quispe, C.A. Ligarda-Samanez, A.M. Solano-Reynoso, B.S. Ramos-Pacheco, Y. Quispe-Quispe, Y. Choque-Quispe, Kari-Ferro, A.J.T.Y.C.D.A., Water quality index in the high-Andean micro-basin of the Chumbao River, Andahuaylas, Apurímac, Peru 12 (2021) 37–73.

[4] A. Quispe-Coica, S. Fernández, L. Acharte Lume, A.J.J. Pérez-Foguet, Status of water quality for human consumption in high-Andean rural communities: Discrepancies between techniques for identifying trace metals 3 (2020) 14, https://doi.org/10.3390/j3020014.

[5] M. Askari Dehno, S.R. Mousavi Harami, M.R. Noora, Environmental geochemistry of heavy metals in coral reefs and sediments of Chabahar Bay, Results in Engineering 13 (2022), 100346, https://doi.org/10.1016/j.rineng.2022.100346.

[6] D.V. Chapman, C. Bradley, G.M. Gettel, I.G. Hatvani, T. Hein, J. Kovács, I. Liska, D. M. Oliver, P. Tanos, B.J.E.S. Trásy, et al., Developments in water quality monitoring and management in large river catchments using the Danube River as an example 64 (2016) 141–154, https://doi.org/10.1016/j.envsci.2016.06.015.

[7] C. Petus, V. Marieu, S. Novoa, G. Chust, N. Bruneau, Froidefond, J.-M.J.C.S.R., Monitoring spatio-temporal variability of the Adour River turbid plume (Bay of Biscay, France) with MODIS 250-m imagery 74 (2014) 35–49, https://doi.org/10.1016/j.csr.2013.11.011.

[8] Y. Liu, B. Zheng, Q. Fu, L. Wang, M.J.P.E.S. Wang, The Selection of Monitoring Indicators for River Water Quality Assessment, vol. 13, 2012, pp. 129–139, https://doi.org/10.1016/j.proenv.2012.01.013.

[9] K. Rani, T. Gomathi, K. Vijayalakshmi, M. Saranya, P.N. Sudha, Banana fiber Cellulose Nano Crystals grafted with butyl acrylate for heavy metal lead (II) removal, Int. J. Biol. Macromol. 131 (2019) 461–472, https://doi.org/10.1016/j.ijbiomac.2019.03.064.

[10] D. Choque-Quispe, C.A. Ligarda-Samanez, B.S. Ramos-Pacheco, A.M. Solano-Reynoso, J. Quispe-Marcatoma, Y. Choque-Quispe, D.E. Peralta-Guevara, E. L. Martínez-Huamán, O. Correa-Cuba, M.L. Masco-Arriola, et al., Formulation of novel composite (activated nanoclay/hydrocolloid of nostoc sphaericum) and its application in the removal of heavy metals from wastewater, Polymers 14 (2022), https://doi.org/10.3390/polym14142803.

[11] A.S. Singha, A. Guleria, Chemical modification of cellulosic biopolymer and its use in removal of heavy metal ions from wastewater, Int. J. Biol. Macromol. 67 (2014) 409–417, https://doi.org/10.1016/j.ijbiomac.2014.03.046.

[12] R.R. Pawar, , Lalhmunsiama, H.C. Bajaj, S.-M. Lee, Activated bentonite as a low-cost adsorbent for the removal of Cu(II) and Pb(II) from aqueous solutions: batch and column studies, J. Ind. Eng. Chem. 34 (2016) 213–223, https://doi.org/10.1016/j.jiec.2015.11.014.

[13] H.S. Ibrahim, N.S. Ammar, M. Soylak, M. Ibrahim, Removal of Cd(II) and Pb(II) from aqueous solution using dried water hyacinth as a biosorbent, Spectrochim. Acta Mol. Biomol. Spectrosc. 96 (2012) 413–420, https://doi.org/10.1016/j.saa.2012.05.039.

[14] M.M. Aljohani, S.D. Al-Qahtani, M. Alshareef, M.G. El-Desouky, A.A. El-Bindary, N. M. El-Metwaly, M.A. El-Bindary, Highly efficient adsorption and removal bio-staining dye from industrial wastewater onto mesoporous Ag-MOFs, Process Saf. Environ. Protect. 172 (2023) 395–407, https://doi.org/10.1016/j.psep.2023.02.036.

[15] T.A. Altalhi, M.M. Ibrahim, G.A.M. Mersal, M.H.H. Mahmoud, T. Kumeria, M.G. El-Desouky, A.A. El-Bindary, M.A. El-Bindary, Adsorption of doxorubicin hydrochloride onto thermally treated green adsorbent: equilibrium, kinetic and thermodynamic studies, J. Mol. Struct. 1263 (2022), 133160, https://doi.org/10.1016/j.molstruc.2022.133160.

[16] K. Rajeshwari, S. Latha, T. Gomathi, K. Sangeetha, P.N. Sudha, Adsorption of heavy metal Cr (VI) by a ternary biopolymer blend, Mater. Today: Proc. 5 (2018) 14628–14638, https://doi.org/10.1016/j.matpr.2018.03.054.

[17] L. Largitte, R. Pasquier, A review of the kinetics adsorption models and their application to the adsorption of lead by an activated carbon, Chem. Eng. Res. Des. 109 (2016) 495–504, https://doi.org/10.1016/j.cherd.2016.02.006.

[18] C.A. Ligarda-Samanez, D. Choque-Quispe, H. Palomino-Rincón, B.S. Ramos-Pacheco, E. Moscoso-Moscoso, M.L. Huamán-Carrión, D.E. Peralta-Guevara, M. E. Obregón-Yupanqui, J. Aroni-Huamán, E.Y. Bravo-Franco, et al., Modified polymeric biosorbents from rumex acetosella for the removal of heavy metals in wastewater, Polymers 14 (2022), https://doi.org/10.3390/polym14112191.

[19] E.O. Oyelude, J.A.M. Awudza, S.K. Twumasi, Removal of malachite green from aqueous solution using pulverized teak leaf litter: equilibrium, kinetic and thermodynamic studies, Chem. Cent. J. 12 (2018) 81, https://doi.org/10.1186/s13065-018-0448-8.

[20] S. Kokate, K. Parasuraman, H. Prakash, Adsorptive removal of lead ion from water using banana stem scutcher generated in fiber extraction process, Results in Engineering 14 (2022), 100439, https://doi.org/10.1016/j.rineng.2022.100439.

[21] A.O. Okewale, K.A. Babayemi, A.P. Olalekan, Adsorption isotherms and kinetics models of starchy adsorbents on uptake of water from ethanol–water systems, Int. J. Appl. Sci. Technol. 3 (2013) 35–42.

[22] G.-N. Moroi, E. Avram, L. Bulgariu, Adsorption of heavy metal ions onto surface-functionalised polymer beads. I. Modelling of equilibrium isotherms by using non-linear and linear regression analysis, Water, Air, Soil Pollut. 227 (2016) 260, https://doi.org/10.1007/s11270-016-2953-5.

[23] Q. Chen, Y. Zhao, Q. Xie, C. Liang, Z. Zong, Polyethyleneimine grafted starch nanocrystals as a novel biosorbent for efficient removal of methyl blue dye, Carbohydr. Polym. 273 (2021), 118579, https://doi.org/10.1016/j.carbpol.2021.118579.

[24] M. Naushad, T. Ahamad, G. Sharma, A.a.H. Al-Muhtaseb, A.B. Albadarin, M. M. Alam, Z.A. Alothman, S.M. Alshehri, A.A. Ghfar, Synthesis and characterization of a new starch/SnO2 nanocomposite for efficient adsorption of toxic Hg2+ metal ion, Chem. Eng. J. 300 (2016) 306–316, https://doi.org/10.1016/j.cej.2016.04.084.

[25] X. Ma, X. Liu, D.P. Anderson, P.R. Chang, Modification of porous starch for the adsorption of heavy metal ions from aqueous solution, Food Chem. 181 (2015) 133–139, https://doi.org/10.1016/j.foodchem.2015.02.089.

[26] S.V. Vargas-Solano, F. Rodríguez-González, R. Martínez-Velarde, S.S. Morales-García, M.P. Jonathan, Removal of heavy metals present in water from the Yautepec River Morelos México, using Opuntia ficus-indica mucilage, Environmental Advances 7 (2022), 100160, https://doi.org/10.1016/j.envadv.2021.100160.

[27] M. Onditi, A.A. Adelodun, E.O. Changamu, J.C. Ngila, Removal of Pb2+ and Cd2+ from drinking water using polysaccharide extract isolated from cactus pads (Opuntia ficus indica), J. Appl. Polym. Sci. 133 (2016), https://doi.org/10.1002/app.43913.

[28] A. Farahnaky, B. Saberi, M. Majzoobi, Effect of glycerol on physical and mechanical properties of wheat starch edible films, J. Texture Stud. 44 (2013) 176–186, https://doi.org/10.1111/jtxs.12007.

[29] D. Choque-Quispe, Y. Diaz-Barrera, A.M. Solano-Reynoso, Y. Choque-Quispe, B. S. Ramos-Pacheco, C.A. Ligarda-Samanez, D.E. Peralta-Guevara, E.L. Martínez-Huamán, J.P. Aguirre Landa, O. Correa-Cuba, et al., Effect of the application of a coating native potato starch/nopal mucilage/pectin on physicochemical and physiological properties during storage of fuerte and hass avocado (persea americana), Polymers 14 (2022), https://doi.org/10.3390/polym14163421.

[30] Y.S. Murillo, L. Giraldo, J.C. Moreno, Determination of the 2, 4-dinitrofenol adsorption kinetic on bovine bone char by UV-Vis spectrophotometry, Rev. Colomb. Quím. 40 (2011) 91–103.

[31] S.A. Drweesh, N.A. Fathy, M.A. Wahba, A.A. Hanna, A.I.M. Akarish, E.A. M. Elzahany, I.Y. El-Sherif, K.S. Abou-El-Sherbini, Equilibrium, kinetic and thermodynamic studies of Pb(II) adsorption from aqueous solutions on HCl-treated Egyptian kaolin, J. Environ. Chem. Eng. 4 (2016) 1674–1684, https://doi.org/10.1016/j.jece.2016.02.005.

[32] S.H. Chien, W.R. Clayton, Application of Elovich equation to the kinetics of phosphate release and sorption in soils, Soil Sci. Soc. Am. J. 44 (1980) 265–268, https://doi.org/10.2136/sssaj1980.03615995004400020013x.

[33] F. Zhang, X. Tang, Y. Huang, A.A. Keller, J. Lan, Competitive removal of Pb2+ and malachite green from water by magnetic phosphate nanocomposites, Water Res. 150 (2019) 442–451, https://doi.org/10.1016/j.watres.2018.11.057.

[34] Y. Zhou, J. Lu, Y. Zhou, Y. Liu, Recent advances for dyes removal using novel adsorbents: a review, Environ. Pollut. 252 (2019) 352–365, https://doi.org/10.1016/j.envpol.2019.05.072.

[35] I. Langmuir, The adsorption of gases on plane surfaces of glass, mica and platinum, J. Am. Chem. Soc. 40 (1918) 1361–1403, https://doi.org/10.1021/ja02242a004.

[36] D. Saravanan, T. Gomathi, P.N. Sudha, Sorption studies on heavy metal removal using chitin/bentonite biocomposite, Int. J. Biol. Macromol. 53 (2013) 67–71, https://doi.org/10.1016/j.ijbiomac.2012.11.005.

[37] M.K. Seliem, S. Komarneni, T. Byrne, F.S. Cannon, M.G. Shahien, A.A. Khalil, I. M. Abd El-Gaid, Removal of nitrate by synthetic organosilicas and organoclay: kinetic and isotherm studies, Separ. Purif. Technol. 110 (2013) 181–187, https://doi.org/10.1016/j.seppur.2013.03.023.

[38] P. Ramachandran, R. Vairamuthu, S. Ponnusamy, Adsorption isotherms, kinetics, thermodynamics and desorption studies of reactive Orange 16 on activated carbon derived from Ananas comosus (L.) carbon, J. Eng. Appl. Sci. 6 (2011) 15–26.

[39] M.A. Hossain, H.H. Ngo, W.S. Guo, T.V. Nguyen, Palm oil fruit shells as biosorbent for copper removal from water and wastewater: experiments and sorption models, Bioresour. Technol. 113 (2012) 97–101, https://doi.org/10.1016/j.biortech.2011.11.111.

[40] P. Senthil Kumar, S. Ramalingam, C. Senthamarai, M. Niranjanaa, P. Vijayalakshmi, S. Sivanesan, Adsorption of dye from aqueous solution by cashew nut shell: studies on equilibrium isotherm, kinetics and thermodynamics of interactions, Desalination 261 (2010) 52–60, https://doi.org/10.1016/j.desal.2010.05.032.

[41] T. Said, Kinetics, thermodynamics, equilibrium, surface modelling, and atomic absorption analysis of selective Cu(ii) removal from aqueous solutions and rivers water using silica-2-(pyridin-2-ylmethoxy)ethan-1-ol hybrid material, RSC Adv. 12 (2021) 611–625, https://doi.org/10.1039/d1ra06640d, 2021.

[42] U.R. Lakshmi, V.C. Srivastava, I.D. Mall, D.H. Lataye, Rice husk ash as an effective adsorbent: evaluation of adsorptive characteristics for Indigo Carmine dye, J. Environ. Manag. 90 (2009) 710–720, https://doi.org/10.1016/j.jenvman.2008.01.002.

[43] S. Rangabhashiyam, N. Anu, M.S. Giri Nandagopal, N. Selvaraju, Relevance of isotherm models in biosorption of pollutants by agricultural byproducts, J. Environ. Chem. Eng. 2 (2014) 398–414, https://doi.org/10.1016/j.jece.2014.01.014.
[44] T.V.N. Padmesh, K. Vijayaraghavan, G. Sekaran, M. Velan, Application of two-and three-parameter isotherm models: biosorption of acid red 88 onto Azolla microphylla, Ann. Finance 10 (2006) 37–44, https://doi.org/10.1080/10889860600842746.
[45] I. Emiola, R. Adem, Comparison of minimization methods for Rosenbrock functions, in: Proceedings of the 2021 29th Mediterranean Conference on Control and Automation, (MED), 2021, pp. 837–842, 22-25 June 2021.
[46] P. Novati, Some secant approximations for Rosenbrock W-methods, Appl. Numer. Math. 58 (2008) 195–211, https://doi.org/10.1016/j.apnum.2006.11.007.
[47] G.F. El-Said, M.M. El-Sadaawy, M.A. Aly-Eldeen, Adsorption isotherms and kinetic studies for the defluoridation from aqueous solution using eco-friendly raw marine green algae, Ulva lactuca, Environ. Monit. Assess. 190 (2017) 14, https://doi.org/10.1007/s10661-017-6392-6.
[48] C. Balan, B. Robu, P. Bulai, D.J.E.E. Bilba, M. Journal, Modeling equilibrium data for Cd (II) adsorption by peat using non-linear regression analysis 16 (2017), https://doi.org/10.30638/eemj.2017.058.
[49] L.T. Popoola, A.S. Yusuff, O.A. Adesina, , Lala, M.A.J.J.o.E.S., Technology, Brilliant green dye sorption onto snail shell-rice husk: statistical and error function models as parametric isotherm predictors 12 (2019) 65–80.
[50] K.Y. Foo, B.H. Hameed, Insights into the modeling of adsorption isotherm systems, Chem. Eng. J. 156 (2010) 2–10, https://doi.org/10.1016/j.cej.2009.09.013.
[51] D.C. González Sandoval, B. Luna Sosa, G.C. Martínez-Ávila, H. Rodríguez Fuentes, V.H. Avendaño Abarca, R. Rojas, Formulation and characterization of edible films based on organic mucilage from Mexican opuntia ficus-indica, Coatings 9 (2019), https://doi.org/10.3390/coatings9080506.
[52] A. Galindez, L.D. Daza, A. Homez-Jara, V.S. Eim, H.A. Váquiro, Characterization of ulluco starch and its potential for use in edible films prepared at low drying temperature, Carbohydr. Polym. 215 (2019) 143–150, https://doi.org/10.1016/j.carbpol.2019.03.074.
[53] A.Y. Guadarrama-Lezama, J. Castaño, G. Velázquez, H. Carrillo-Navas, J. Alvarez-Ramírez, Effect of nopal mucilage addition on physical, barrier and mechanical properties of citric pectin-based films, J. Food Sci. Technol. 55 (2018) 3739–3748, https://doi.org/10.1007/s13197-018-3304-x.
[54] T. Todhanakasem, P. Boonchuai, P. Itsarangkoon Na Ayutthaya, R. Suwapanich, B. Hararak, B. Wu, B.M. Young, Development of bioactive opuntia ficus-indica edible films containing probiotics as a coating for fresh-cut fruit, Polymers 14 (2022), https://doi.org/10.3390/polym14225018.
[55] D.F. Apopei, M.V. Dinu, A.W. Trochimczuk, E.S. Dragan, Sorption isotherms of heavy metal ions onto semi-interpenetrating polymer network cryogels based on polyacrylamide and anionically modified potato starch, Ind. Eng. Chem. Res. 51 (2012) 10462–10471, https://doi.org/10.1021/ie301254z.
[56] A. Bashir, T. Manzoor, L.A. Malik, A. Qureashi, A.H. Pandith, Enhanced and selective adsorption of Zn(II), Pb(II), Cd(II), and Hg(II) ions by a dumbbell- and flower-shaped potato starch phosphate polymer: a combined experimental and dft calculation study, ACS Omega 5 (2020) 4853–4867, https://doi.org/10.1021/acsomega.9b03607.
[57] J. Kollannur Nikhil, N. Arnepalli Dali, Methodology for determining point of zero salt effect of clays in terms of surface charge properties, J. Mater. Civ. Eng. 31 (2019), 04019286, https://doi.org/10.1061/(ASCE)MT.1943-5533.0002947.
[58] M. Çakmak, Ş. Taşar, V. Selen, D. Özer, A. Özer, Removal of astrazon golden yellow 7GL from colored wastewater using chemically modified clay, J. Cent. S. Univ. 24 (2017) 743–753, https://doi.org/10.1007/s11771-017-3476-y.
[59] A.H. Zyoud, A. Zubi, S.H. Zyoud, M.H. Hilal, S. Zyoud, N. Qamhieh, A. Hajamohideen, H.S. Hilal, Kaolin-supported ZnO nanoparticle catalysts in self-sensitized tetracycline photodegradation: zero-point charge and pH effects, Appl. Clay Sci. 182 (2019), 105294, https://doi.org/10.1016/j.clay.2019.105294.
[60] A.-M. Stanescu, L. Stoica, C. Constantin, I. Lacatusu, O. Oprea, F. Miculescu, Physicochemical characterization and use of heat pretreated commercial instant dry baker's yeast as a potential biosorbent for Cu(II) removal, Clean: Soil, Air, Water 42 (2014) 1632–1641, https://doi.org/10.1002/clen.201300484.
[61] L.L. Schramm, Emulsions, Foams, Suspensions, and Aerosols: Microscience and Applications, John Wiley & Sons, 2014.
[62] V.t. Quyen, T.-H. Pham, J. Kim, D.M. Thanh, P.Q. Thang, Q. Van Le, S.H. Jung, T. Kim, Biosorbent derived from coffee husk for efficient removal of toxic heavy metals from wastewater, Chemosphere 284 (2021), 131312, https://doi.org/10.1016/j.chemosphere.2021.131312.
[63] D. Choque-Quispe, Y. Choque-Quispe, C.A. Ligarda-Samanez, D.E. Peralta-Guevara, A.M. Solano-Reynoso, B.S. Ramos-Pacheco, F. Taipe-Pardo, E. L. Martínez-Huamán, J.P. Aguirre Landa, H.W. Agreda Cerna, et al., Effect of the addition of corn husk cellulose nanocrystals in the development of a novel edible film, Nanomaterials 12 (2022), https://doi.org/10.3390/nano12193421.
[64] K. Aftab, S. Hameed, H. Umbreen, S. Ali, M. Rizwan, S. Alkahtani, M.M. Abdel-Daim, Physicochemical and functional potential of hydrocolloids extracted from some solanaceae plants, J. Chem. 2020 (2020), 3563945, https://doi.org/10.1155/2020/3563945.
[65] V. Sessini, M.P. Arrieta, J.M. Kenny, L. Peponi, Processing of edible films based on nanoreinforced gelatinized starch, Polym. Degrad. Stabil. 132 (2016) 157–168, https://doi.org/10.1016/j.polymdegradstab.2016.02.026.
[66] E. Basiak, A. Lenart, F. Debeaufort, How glycerol and water contents affect the structural and functional properties of starch-based edible films, Polymers 10 (2018), https://doi.org/10.3390/polym10040412.
[67] M.H.G. Canteri, C.M.G.C. Renard, C. Le Bourvellec, S. Bureau, ATR-FTIR spectroscopy to determine cell wall composition: application on a large diversity of fruits and vegetables, Carbohydr. Polym. 212 (2019) 186–196, https://doi.org/10.1016/j.carbpol.2019.02.021.
[68] C. Liu, S. Jiang, S. Zhang, T. Xi, Q. Sun, L. Xiong, Characterization of edible corn starch nanocomposite films: the effect of self-assembled starch nanoparticles, Starch - Stärke 68 (2016) 239–248, https://doi.org/10.1002/star.201500252.
[69] A. Valdés, C. Martínez, M.C. Garrigos, A. Jimenez, Multilayer films based on poly (lactic acid)/gelatin supplemented with cellulose nanocrystals and antioxidant extract from almond shell by-product and its application on hass avocado preservation, Polymers 13 (2021), https://doi.org/10.3390/polym13213615.
[70] Y.W. Chen, H.V. Lee, J.C. Juan, S.-M. Phang, Production of new cellulose nanomaterial from red algae marine biomass Gelidium elegans, Carbohydr. Polym. 151 (2016) 1210–1219, https://doi.org/10.1016/j.carbpol.2016.06.083.
[71] Y. Zhang, W. Liu, M. Xu, F. Zheng, M. Zhao, Study of the mechanisms of Cu2+ biosorption by ethanol/caustic-pretreated baker's yeast biomass, J. Hazard Mater. 178 (2010) 1085–1093, https://doi.org/10.1016/j.jhazmat.2010.02.051.
[72] D.I. Fox, D.M. Stebbins, N.A. Alcantar, Combining ferric salt and cactus mucilage for arsenic removal from water, Environ. Sci. Technol. 50 (2016) 2507–2513, https://doi.org/10.1021/acs.est.5b04145.
[73] N. Adjeroud-Abdellatif, Y. Hammoui, A. Boudria, S. Agab, F. Choulak, J.-P. Leclerc, B. Merzouk, K. Madani, Effect of a natural coagulant extract from Opuntia ficus-indica cladode on electrocoagulation-electroflotation water treatment process, Int. J. Environ. Anal. Chem. 102 (2022) 5822–5846, https://doi.org/10.1080/03067319.2020.1804889.
[74] M. Khotimchenko, K. Makarova, E. Khozhaenko, V. Kovalev, Lead-binding capacity of calcium pectates with different molecular weight, Int. J. Biol. Macromol. 97 (2017) 526–535, https://doi.org/10.1016/j.ijbiomac.2017.01.065.
[75] I. Matsukevich, Y. Lipai, V. Romanovski, Cu/MgO and Ni/MgO composite nanoparticles for fast, high-efficiency adsorption of aqueous lead(II) and chromium (III) ions, J. Mater. Sci. 56 (2021) 5031–5040, https://doi.org/10.1007/s10853-020-05593-4.
[76] H. Wang, Y. Wang, Z. Liu, S. Luo, V. Romanovski, X. Huang, B. Czech, H. Sun, T. Li, Rational construction of micron-sized zero-valent iron/graphene composite for enhanced Cr(VI) removal from aqueous solution, J. Environ. Chem. Eng. 10 (2022), 109004, https://doi.org/10.1016/j.jece.2022.109004.
[77] A. Hashem, A. Al-Anwar, N.M. Nagy, D.M. Hussein, S. Eisa, Isotherms and kinetic studies on adsorption of Hg(II) ions onto Ziziphus spina-christi L. from aqueous solutions 5 (2016) 213–224, https://doi.org/10.1515/gps-2015-0103.
[78] N.V. Efimova, A.P. Krasnopyorova, G.D. Yuhno, A.A.J.A.S. Scheglovskaya, Technology, Sorption of heavy metals by natural biopolymers 35 (2017) 595–601.
[79] B. Abbou, I. Lebkiri, H. Ouaddari, L. Kadiri, A. Ouass, A. Habsaoui, A. Lebkiri, E. H. Rifi, Removal of Cd(II), Cu(II), and Pb(II) by adsorption onto natural clay: a kinetic and thermodynamic study, Turk. J. Chem. 45 (2021) 362–376, https://doi.org/10.3906/kim-2004-82.
[80] J. Wang, W. Zhang, Evaluating the adsorption of Shanghai silty clay to Cd(II), Pb (II), As(V), and Cr(VI): kinetic, equilibrium, and thermodynamic studies, Environ. Monit. Assess. 193 (2021) 131, https://doi.org/10.1007/s10661-021-08904-7.
[81] S. Selambakkannu, N.A.F. Othman, K.A. Bakar, S.A. Shukor, Z.A. Karim, A kinetic and mechanistic study of adsorptive removal of metal ions by imidazole-functionalized polymer graft banana fiber, Radiat. Phys. Chem. 153 (2018) 58–69, https://doi.org/10.1016/j.radphyschem.2018.09.012.
[82] G. De Angelis, L. Medeghini, A.M. Conte, S. Mignardi, Recycling of eggshell waste into low-cost adsorbent for Ni removal from wastewater, J. Clean. Prod. 164 (2017) 1497–1506, https://doi.org/10.1016/j.jclepro.2017.07.085.
[83] E.-S.R.E. Hassan, M. Rostom, F.E. Farghaly, M.A. Abdel Khalek, Bio-sorption for tannery effluent treatment using eggshell wastes; kinetics, isotherm and thermodynamic study, Egyptian Journal of Petroleum 29 (2020) 273–278, https://doi.org/10.1016/j.ejpe.2020.10.002.
[84] A. Esmaeili, N. Khoshnevisan, Optimization of process parameters for removal of heavy metals by biomass of Cu and Co-doped alginate-coated chitosan nanoparticles, Bioresour. Technol. 218 (2016) 650–658, https://doi.org/10.1016/j.biortech.2016.07.005.
[85] M. Šuránek, Z. Melichová, V. Kureková, L. Kljajević, S. Nenadović, Removal of nickel from aqueous solutions by natural bentonites from Slovakia, Materials 14 (2021), https://doi.org/10.3390/ma14020282.
[86] B. Kozera-Sucharda, B. Gworek, I. Kondzielski, J. Chojnicki, The comparison of the efficacy of natural and synthetic aluminosilicates, including zeolites, in concurrent elimination of lead and copper from multi-component aqueous solutions, Processes 9 (2021), https://doi.org/10.3390/pr9050812.
[87] B. Kozera-Sucharda, B. Gworek, I. Kondzielski, The simultaneous removal of zinc and cadmium from multicomponent aqueous solutions by their sorption onto selected natural and synthetic zeolites, Minerals 10 (2020), https://doi.org/10.3390/min10040343.
[88] C.C. Nnaji, A.E. Agim, C.N. Mama, P.C. Emenike, N.M.J.S.R. Ogarekpe, Equilibrium and thermodynamic investigation of biosorption of nickel from water by activated carbon made from palm kernel chaff 11 (2021) 1–20.
[89] D. Saravanan, Sudha, P.J.I.J.o.C.R., Batch adsorption studies for the removal of copper from wastewater using natural biopolymer 6 (2014) 3496–3508.
[90] F.-C. Wu, B.-L. Liu, K.-T. Wu, R.-L. Tseng, A new linear form analysis of Redlich–Peterson isotherm equation for the adsorptions of dyes, Chem. Eng. J. 162 (2010) 21–27, https://doi.org/10.1016/j.cej.2010.03.006.

[91] N. Ayawei, A.N. Ebelegi, D. Wankasi, Modelling and interpretation of adsorption isotherms, J. Chem. 2017 (2017), 3039817, https://doi.org/10.1155/2017/3039817.

[92] H.A. Kiwaan, , Sh. Mohamed, F., A.A. El-Bindary, N.A. El-Ghamaz, H.R. Abo-Yassin, M.A. El-Bindary, Synthesis, identification and application of metal organic framework for removal of industrial cationic dyes, J. Mol. Liq. 342 (2021), 117435, https://doi.org/10.1016/j.molliq.2021.117435.

[93] H.A. Kiwaan, F.S. Mohamed, N.A. El-Ghamaz, N.M. Beshry, A.A. El-Bindary, Experimental and electrical studies of Na-X zeolite for the adsorption of different dyes, J. Mol. Liq. 332 (2021), 115877, https://doi.org/10.1016/j.molliq.2021.115877.